Journal of Magnetic Resonance **149,** 234–238 (2001)
doi:10.1006/jmre.2001.2306, available online at http://www.idealibrary.com on IDEAL®

Delayed-Focus Pulses Optimized Using Simulated Annealing

Jun Shen

The Nathan S. Kline Institute, Orangeburg, New York 10962

Received November 7, 2000; revised January 30, 2001; published online April 2, 2001

Unlike prefocused pulses and shaped pulses based on the linear response theory, delayed-focus pulses (X.-L. Wu *et al.*, 1991, *Magn. Reson. Med.* 20, 165–170) produce a selective spin echo after a predefined short delay without using a π refocusing pulse. In this paper, a series of delayed-focus pulses of different flip angles are proposed based on optimization using Fourier series representation and simulated annealing. The resistance of these delayed-focus pulses to T_2 relaxation is also demonstrated using numerical simulation of Bloch equations.

Key Words: **shaped pulses; linear response; delayed focus; spin echo; T_2 relaxation.**

INTRODUCTION

Under the assumption of the linear response theory the induced magnetization is proportional to the resonant Fourier component of the applied field. For RF pulses designed based on the linear response theory (e.g., Gaussian and sinc pulses) the center of time for evolution of magnetization $t_0 = T_p/2$ when they act on equilibrium magnetization, where T_p is the duration of the pulse. These RF pulses result in a characteristic approximately linear phase roll across the excited spectral region in accordance with the shift theorem (*1*). For magnetic resonance imaging applications the unwanted evolution of magnetization during a Gaussian or sinc pulse can be refocused by a gradient reversal following the RF pulse. Since the evolution of chemical shift during a RF pulse cannot be refocused by a gradient pulse great efforts have been made to design the so-called "prefocused" or "self-refocused" RF pulses which result in an approximately zero phase immediately after the pulse (*2, 3*). In this case the center of time for magnetization evolution $t_0 = T_p$. Prefocused pulses have found many applications in both high-resolution and *in vivo* NMR spectroscopy (*4, 5*). They also have found important applications in magnetic resonance imaging, especially the prefocused 180° slice-selective refocusing pulses (*6, 7*).

Using an evolutionary approach, Wu *et al.* (*8*) proposed a class of delayed-focus pulses which generate a 90° excitation of a selective spin-echo. The spin-echo pulses proposed by Pauly *et al.* (*9, 10*) optimized using the SLR algorithm also have a delayed focus where a selective spin echo is produced. In both cases, the B_0 field gradient and chemical shifts are refocused by these RF pulses. Therefore, within the selected spectral window, an approximate zero phase is produced at $t_0 = T_p + \Delta t$, where Δt is a predefined short delay. As pointed out by Wu *et al.* (*8*) and by Pauly and Macovski (*9*), these pulses should be very useful for magnetic resonance imaging experiments because no reversal of the slice-selection gradient is needed while phase-encoding gradients can be applied during the extra delay Δt. However, to apply these pulses to magnetic resonance imaging a series of delayed-focus or spin-echo pulses with various flip angles, low RF power requirement, and excellent resistance to relaxation have to be generated. In this paper we use the combined Fourier series representation and simulated annealing technique to produce a series of RF pulses with flip angles of 30°, 45°, 60°, and 90° which generate a selective spin echo at $\Delta t/T_p = 0.125$. The RF power requirement of these pulses is similar to that of an E-BURP-1 pulse (*2*). These pulses also show excellent resistance to degradation caused by T_2 relaxation.

METHODS

RF Pulse Optimization

The delayed-focus pulses (hereafter referred to as DFP pulses) were designed to be amplitude-modulated with their shapes defined by a finite Fourier series (*2*),

$$\gamma B_1(t) = \omega \sum_{n=1}^{m} [A_n \cos(n\omega t) + B_n \sin(n\omega t)], \qquad [1]$$

where $\omega = 2\pi/T_p$, and A_n and B_n are Fourier coefficients to be determined to generate a selective spin echo at $T_p + \Delta t$.

A simulated annealing algorithm was implemented on a SPARCStation 20 computer to search for the optimal pulse shapes for a predefined $\Delta t/T_p$ ratio and a predefined spin-echo profile at $T_p + \Delta t$. The starting Fourier coefficients ($m = 5$–10) were set to zero except for A_0 which was set to $\alpha/2\pi$ as required by Eq. [1], where α is the pulse flip angle in radians. Pulse shape calculated from the finite Fourier series was digitized into 64 or 256 segments. At $t = 0$, $M_x = M_y = 0$, $M_z = M_0$, where M_0 is the equilibrium magnetization. For each RF pulse segment matrix multiplication based on Bloch equations without the relaxation terms was performed to calculate the sequential rotation

1090-7807/01 $35.00

of the magnetization by each digitized RF segment. For the time interval $T_p \sim T_p + \Delta t$, $\gamma B_1 = 0$, the magnetization evolves only under the influence of resonance offset. The mean square deviation of the magnetization profile at $t = T_p + \Delta t$ was evaluated for the following predefined target profile,

$$\begin{aligned} &M_y(\upsilon) = \sin\alpha,\ M_x(\upsilon) = 0, && \text{for } \upsilon = 0 \sim 1.5/T_p \\ &M_x(\upsilon) = 0, && \text{for } \upsilon = 2/T_p \sim 2.5/T_p \\ &M_y(\upsilon) = 0,\ M_x(\upsilon) = 0, && \text{for } \upsilon = 3/T_p \sim 10/T_p, \end{aligned}$$

where υ is the resonance offset in hertz. The target profile was evaluated at intervals of $0.5/T_p$. The initial temperature of the Metropolis algorithm (*11, 12*) was set to generate an uphill success ratio of ~100%. The annealing schedule used was $T_i/T_{i-1} = 0.9 \sim 0.95$. For each temperature step, the maximum number of attempted uphill moves and successful uphill moves was set to be 500 and 50 per Fourier coefficient, respectively. One set of Fourier coefficients corresponding to the minimum mean square deviation with respect to a predefined flip angle, a predefined $\Delta t/T_p$ ratio, and the designated spin-echo profile was obtained after each annealing run.

Simulation of T_2 Relaxation

The effect of T_2 relaxation during the DFP pulses and Δt on selectivity and signal intensity was simulated by numerically integrating the Bloch equations including the T_2 relaxation terms (*13*). The magnitudes of the on-resonance spin echo generated by the delayed-focus pulses and other RF pulses (*1, 2*) under varying T_2 were fitted to a single exponential decay (*14, 15*),

$$M = M_0 \sin\alpha \exp\left(-\frac{\tau}{T_2}\right), \qquad [2]$$

where τ, the effective time of echo (TE) with respect to T_2 relaxation, is equivalent to the TE of a hard pulse spin-echo sequence that generates the same T_2 relaxation effects.

RESULTS

Figure 1 shows a series of 90° delayed-focus RF pulses with various predefined $\Delta t/T_p$ ratios: 0 (equivalent to E-BURP-1), 0.25/4.0, 0.5/4.0, and 0.75/4.0. The pulse shapes were obtained using the combined Fourier representation and simulated annealing method as described under Methods. The peak amplitude of the pulses exhibits a minimum at $\Delta t/T_p = 0.125$. For $T_p = 4$ ms (bandwidth = 1125 Hz), $\Delta t = 0.5$ ms. The corresponding 90° delayed-focus pulse (DFP90) requires a B_1 peak amplitude of 831 Hz, which is comparable to that of the E-BURP-1 pulse. For $\Delta t/T_p > 0.75/4.0$, the selectivity of the spin-echo profile deviates significantly from the target excitation profile while both the peak power and the integrated power increase further.

The pulse ordinates for delayed-focus pulses with flip angles of 30°, 45°, 60°, and 90° are plotted in Fig. 2. $\Delta t/T_p = 0.125$ for all flip angles. Their peak amplitude requirements are listed in Table 1. Figure 3 demonstrates the evolution of the excitation profiles obtained at $\Delta t = 0$, 0.25, 0.5, and 0.75 ms using a 4-ms 90° delayed-focus pulse (DFP90, designed for $\Delta t/T_p = 0.125$). Clearly, the delayed-focus pulse generates a "focused" selective spin echo at $\Delta t = 0.5$ ms. The achieved phase purity at the refocusing point for DFP pulses is similar to that of the E-BURP-1 pulse at $\Delta t = 0$ (2). Simulation of a five-lobe sinc pulse ($t_0 = T_p/2$) and an E-BURP-1 pulse ($t_0 = T_p$) confirmed that they are not suitable for spin-echo generation at $T_p + \Delta t$.

Figure 4 shows a one-dimensional spin-echo profile of a DFP90 pulse using a 10-cm-diameter spherical water phantom and a 3.0T SMIS spectrometer (Surrey Medical Systems,

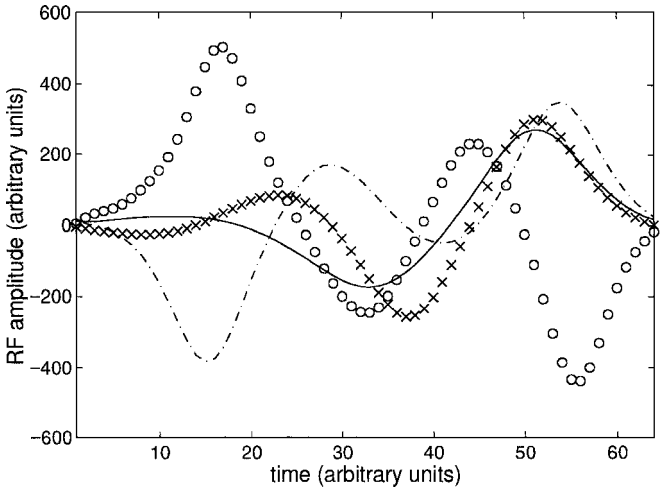

FIG. 1. Pulse ordinates for $\alpha = 90°$, $\Delta t/T_p = 0$ (E-BURP-1, cross), 0.25/4.0 (dotted-dashed line), 0.5/4.0 (DFP90, solid line), and 0.75/4.0 (open circle).

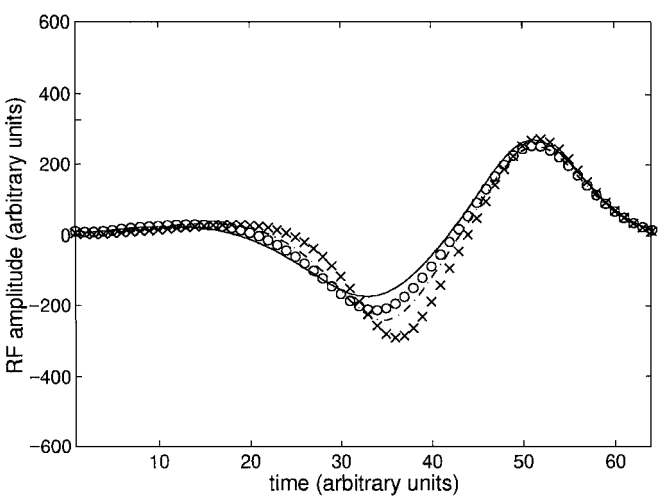

FIG. 2. Pulse ordinates for $\alpha = 30°$ (DFP30, cross),* 45° (DFP45, dotted-dashed line), 60° (DFP60, open circles), and 90° (DFP90, solid line). $\Delta t/T_p = 0.125$ for all pulses. *Fourier coefficients: A_n = 0.086, 1.529, −1.298, −0.230, 0.041, 0.022, 0.055, −0.036, 0.003, −0.004; B_n = 0.000, −0.456, −1.235, 0.656, −0.028, 0.100, −0.064, −0.013, 0.002, −0.003.

TABLE 1
RF Peak Amplitude and Effective Relaxation TE

RF pulse	Peak amplitude $\times T_p$[a]	Effective TE / $(T_p + \Delta t)$[b]
Five-lobe sinc	1.4	0.56
E-BURP-1	3.7	0.44
DFP30	3.6	0.49
DFP45	3.1	0.51
DFP60	3.1	0.49
DFP90	3.3	0.47

[a] Peak amplitude is in Hz, and T_p is in s.
[b] Effective relaxation TE ($=\tau$ in Eq. [2]), and $\Delta t / T_p = 0.125$.

Guilford, UK). The test sequence consists of a 4-ms DFP90 pulse to select a 1-cm axial slice and a subsequent gradient echo along the *z* axis for readout. A 0.5-ms refocusing gradient of the *same* polarity as that of the slice-selection gradient was used after the DFP90 pulse. The area of the refocusing gradient was set to 0.5 ms times the amplitude of slice-selection gradient. The acquired phase-sensitive slice profile shows a full slice-selective 90° excitation as expected. The phase purity at $t = T_p + \Delta t$ was also confirmed by using the same DFP90 pulse ($T_p + \Delta t = 4.5$ ms) to excite bulk water while shifting the transmitter frequency over a frequency range covering ±2000 Hz.

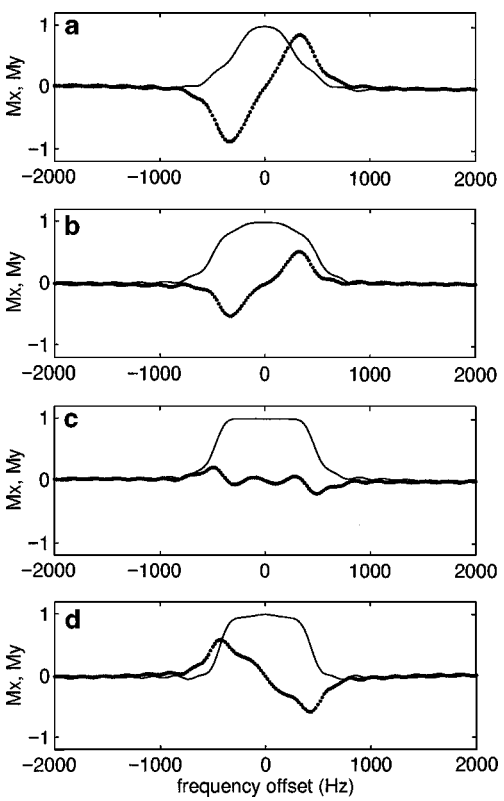

FIG. 3. Comparison of spin-echo profiles generated by a 4-ms DFP90 pulse at (a) 0 ms, (b) 0.25 ms, (c) 0.5 ms, and (d) 0.75 ms after the pulses. Similar results were also obtained for the DFP30, DFP45, and DFP60 pulses.

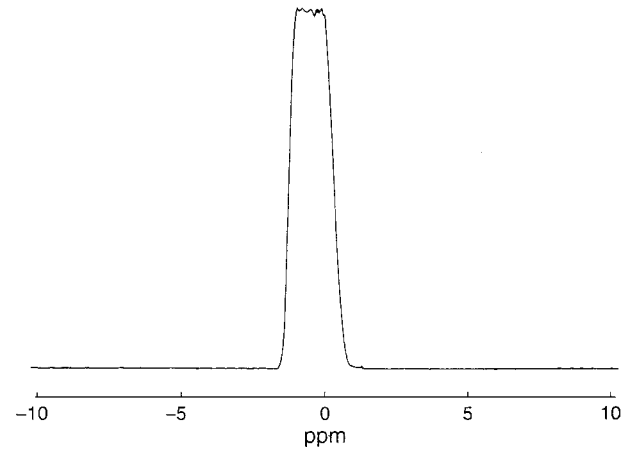

FIG. 4. A phase-sensitive excitation profile generated using a 4-ms DFP90 pulse to select a 1-cm axial slice. A 0.5-ms refocusing gradient of the same polarity as that of the slice-selection gradient was used after the DFP90 pulse. The area of the refocusing gradient was set to be 0.5 ms times the amplitude of slice-selection gradient. A 10-cm water phantom was used for the test.

Results similar to those of E-BURP-1 with $\Delta t = 0$ (*2*) were obtained without adjustment of phase control (data not shown).

Figure 5 shows the simulated pulse excitation profiles generated by a DFP90 pulse ($T_p = 4$ ms, $\Delta t = 0.5$ ms) at $T_2 = 100$ and 20 ms, respectively. T_1 was set to 2 s in each case. Clearly, the degradation of the selectivity of the slice profile under these conditions is negligible. The only significant change is the unavoidable decrease in the magnitude of the selected signal intensity. The magnitude of the on-resonance magnetization under various T_2 relaxation conditions fits to a single exponential (Eq. [2]). The decrease in signal intensity due to relaxation of the transverse components during $T_p + \Delta t$ is shown in Fig. 6. In Eq. [2], τ is

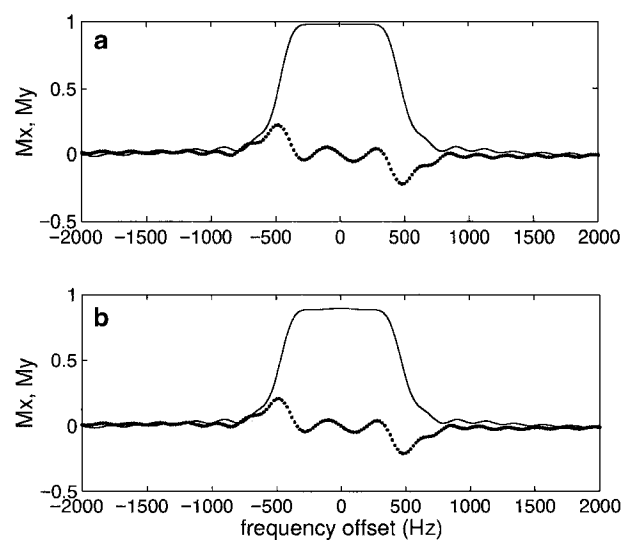

FIG. 5. Simulated spin-echo profiles generated by a 4-ms DFP90 pulse for short T_2 ($T_1 = 2$ s). (a) $T_2 = 100$ ms. (b) $T_2 = 20$ ms. Solid lines are absorptive magnetization; dotted lines are dispersive magnetization. $\Delta t = 0.5$ ms for both cases.

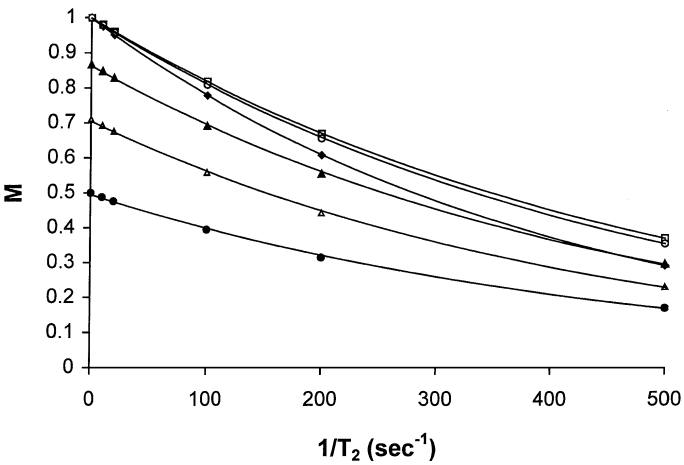

FIG. 6. Plots of the decay of on-resonance magnetization as a function of T_2 ($T_1 = 2$ s). Pulses shown are the following: 90° five-lobe sinc, closed diamonds; E-BURP-1, open squares; DFP90, open circles; DFP60, closed triangles; DFP45, open triangles; DFP30, closed circles.

equivalent to the TE of a hard pulse spin-echo sequence that generates the same T_2 relaxation effects. The $\tau/(T_p + \Delta t)$ ratios for the five-lobe sinc pulse, the E-BURP-1 pulse, and the delayed-focus pulses are also listed in Table 1. As shown in Table 1, the extent of signal attenuation for the DFP pulses is similar to that of the prefocused E-BURP-1 pulse. Note that the effects of short T_2 relaxation times are independent of the absolute value of T_2 or pulse length and are instead dependent only on the ratios of the relaxation time to $T_p + \Delta t$. For example, the effects observed for a pulse length (including Δt) of 5 ms and $T_2 = 20$ ms would be the same for a pulse of 2.5 ms and $T_2 = 10$ ms for the same pulse shape and the same $\Delta t / T_p$.

DISCUSSION

Although not shown under Results the effects of B_1 inhomogeneity on the selectivity of the DFP pulses have also been simulated using Bloch equations. For a ±5% variation in B_1 the degradation of the slice profiles generated by DFP pulses is negligible, similar to that of the E-BURP-1 pulse (*2*). This is because the RF distribution of the DFP pulses is similar to that of the E-BURP-1 pulse, leading to similar tolerance of B_1 inhomogeneity.

Similar to the spin-echo pulses, one potential application of the DFP pulses is in two-dimensional heteronuclear (e.g., ^{31}P, ^{19}F, or ^{13}C) spectroscopic imaging where the phase-encoding gradients can be inserted in the predefined short delay Δt. Due to the short T_2 of many phosphorus components (*16*) chemical shift images of phosphorus-containing metabolites are usually acquired *in vivo* using a simple pulse–acquire scheme with a short delay prior to data sampling to allow for insertion of phase-encoding gradients. The evolution of magnetization during the phase-encoding gradients leads to baseline distortion and therefore complicates metabolite quantitation (*17*). Post-acquisition data processing methods such as backward linear prediction requires high signal-to-noise ratio frequently not accessible in clinical studies. To overcome this difficulty a short-TE spin-echo method using hard pulses (*18*) has been developed for three-dimensional phosphorus chemical shift imaging. An alternative approach would be to apply the concatenated spin-echo pulses or the delayed-focus pulses for two-dimensional spin-echo spectroscopic imaging of phosphorus using the Δt delay prior to acquisition for insertion of phase-encoding gradients.

Since *in vivo* ^{31}P signals have relatively long T_1 values ($\gg$4.5 ms, Ref. (*19*)) only degradation of pulse profiles due to short T_2 relaxation times (*13–15*) is considered here. As shown in Fig. 5 short T_2 relaxation of cerebral phosphorus-containing metabolites under *in vivo* conditions has no appreciable effect on the selectivity of the DFP pulses. This is due to both the short pulse duration achieved ($T_p + \Delta t = 4.5$ ms, RF peak amplitude = 831 Hz for the DFP90 pulse) and the optimal trajectory of the magnetization during the course of RF excitation. The extent of T_2 relaxation during a RF pulse depends on the duration of the pulse and the deviation of the magnetization from equilibrium produced by each increment of the RF pulse ordinate. Using DFP pulses the deviation of magnetization from equilibrium is minimal during the first one-third of the pulse duration. The effective TE ($=\tau$) for T_2 relaxation during the pulse and the extra Δt delay is 2.2 ms for the DFP90 pulse with $T_p = 4$ ms and $\Delta t = 0.5$ ms. Figure 6 demonstrates that the T_2 relaxation during the RF pulses can fit to a single exponential. Therefore, the effective relaxation TE is independent of T_2 differences between different metabolites, which may change under pathological conditions. This will simplify the process of quantification because the effective relaxation TE is identical for all ^{31}P-containing metabolites. The measured signal intensity can be corrected for relaxation loss using T_2 values measured *in vivo*. In the worst cases, e.g., $T_2 = 20$ ms, the T_2 relaxation loss is 10.4% for an effective relaxation TE of 2.2 ms.

Since data acquisition using DFP pulses starts at the center of the spin echo no baseline distortion is expected when applied to heteronuclear chemical shift imaging. Neither the sinc ($t_0 = T_p/2$) nor the prefocused pulse ($t_0 = T_p$) can produce a slice selection and in-phase signals at a predefined delay. This has been verified using numerical simulation with both a five-lobe sinc and an E-BURP-1 pulse causing baseline distortions. Baseline distortion was found to be worst with sinc pulses because the center of time for evolution of magnetization is within the RF pulse per se. No distortion was found for DFP pulses.

Using a single RF pulse to generate a selective spin echo has also been proposed by Pauly and Macovski (*9, 10*). They first used the SLR-based direct design method and obtained a pulse generating a delayed spin echo. Later a series of concatenated spin-echo pulses was optimized using the SLR method (*20*). The first half of the spin-echo pulse performs a prefocused 90° excitation. The second half of the spin-echo pulse performs a prefocused 180° refocusing. Therefore the concatenated pulse can generate a selective spin echo. The optimized spin-echo

pulses have been successfully applied to *in vivo* two-dimensional spectroscopic imaging of phosphomonoesters (PME) and phosphodiesters (PDE) (*20*). In that study, an approximately 6-ms 60° spin-echo pulse (peak RF amplitude = 1000 Hz) was used to generate an echo time of 2.5 ms. The τ value characterizing T_2 loss during the spin echo was not calculated. Using the DFP pulses T_2 loss during the $T_p + \Delta t$ period was significantly reduced due to both the shortened total pulse duration (with lower RF peak amplitude) and the optimal trajectory of magnetization during the early period of the pulse. A further improvement achieved by the DFP pulses is the elimination of phase cycling which is necessary to cancel dispersive magnetization when the concatenated spin-echo pulses are used for slice selection.

Interestingly, the DFP90 optimized by the mechanical simulated annealing routine is very similar to the 90° D-BURP-1 pulses optimized by the much more flexible evolutionary algorithm (*8*). On the other hand, their pulse shapes are very different from that of the 90° D-BURP-2 optimized using the evolutionary method and that of the 90° spin-echo pulses optimized using the SLR method. The D-BURP pulses are all 90° excitation pulses the small flip angle DFP pulses optimized using simulated annealing are all significantly different from the corresponding spin-echo pulses (*20*) which have more complex pulse shapes and also require more RF power.

In conclusion, we have shown that the delayed-focus pulses of various flip angles can be obtained using a combined finite Fourier representation and simulated annealing method. These pulses can be readily applied to *in vivo* magnetic resonance imaging experiments.

ACKNOWLEDGMENTS

The author acknowledges helpful discussions with Dr. Kelvin O. Lim and technical assistance by Mr. Baldev Ahluwalia. This work is supported in part by NIH Grant ROI RR15106 and a NARSAD Young Investigator Award.

REFERENCES

1. C. Bauer, R. Freeman, T. Frenkiel, J. Keeler, and A. J. Shaka, Gaussian pulses, *J. Magn. Reson.* **58,** 442–457 (1984).
2. H. Geen and R. Freeman, Band-selective radiofrequency pulses, *J. Magn. Reson*. **93,** 93–141 (1991).
3. L. Emsley and G. Bodenhausen, Gaussian pulse cascades: New analytical functions for rectangular selective inversion and in-phase excitation in NMR, *Chem. Phys. Lett.* **165,** 469–476 (1990).
4. H. P. Hetherington, J. W. Pan, G. F. Mason, S. L. Ponder, D. B. Twieg, G. Deutsch, J. Mountz, and G. M. Pohost, 2D ^{1}H spectroscopic imaging of the human brain at 4.1 T, *Magn. Reson. Med.* **32,** 530–534 (1994).
5. R. Freeman, Selective excitation in high-resolution NMR, *Chem. Rev.* **91,** 1397–1412 (1991).
6. J. B. Murdoch, A. H. Lent, and M. R. Kritzer, Computer-optimized narrowband pulses for multislice imaging, *J. Magn. Reson.* **74,** 226–263 (1987).
7. L. Emsley and G. Bodenhausen, Optimization of shaped selective pulses for NMR using a quaternion description of their overall propagators, *J. Magn. Reson.* **97,** 135–148 (1992).
8. X.-L. Wu, P. Xu, and R. Freeman, Delayed-focus pulses for magnetic resonance imaging: An evolutionary approach, *Magn. Reson. Med.* **20,** 165–170 (1991).
9. J. Pauly and A. Macovski, Direct design of self-refocusing RF pulses, *in* Abstracts of the Society of Magnetic Resonance in Medicine, 10th Annual Meeting, p. 267 (1991).
10. J. Pauly and A. Macovski, Designing spin echo, *in* Abstracts of the Society of Magnetic Resonance in Medicine, 11th Annual Meeting, p. 3902 (1992).
11. N. Metropolis, A. W. Rosenbluth, M. N. Rosenbluth, A. H. Teller, and E. Teller, Equation of state calculations by fast computing machines. *J. Chem. Phys.* **21,** 1087–1091 (1953).
12. S. Kirkpatrick, C. D. Gelatt, Jr., and M. P. Vecchi, Optimization by simulated annealing, *Science* **220,** 671–680 (1983).
13. D. G. Norris, H. Ludemann, and D. Leibfritz, An analysis of the effects of short T_2 values on the hyperbolic-secant pulse, *J. Magn. Reson.* **92,** 94–101 (1991).
14. P. J. Hajduk, D. A. Horita, and L. E. Lerner, Theoretical analysis of relaxation during shaped pulses. I. The effects of short T_1 and T_2, *J. Magn. Reson. A* **103,** 40–52 (1993).
15. J. Shen and L. E. Lerner, Use of directed simulated annealing to design monochromatic JANUS pulses, *J. Magn. Reson. A* **114,** 116–119 (1995).
16. K. D. Merboldt, D. Chien, H. Bruhn, M. L. Gyngell, W. Hanicke, and J. Frahm, Localized phosphorus NMR spectroscopy of human brain using stimulated echo (STEAM) sequences, *in* Abstracts of the Society of Magnetic Resonance in Medicine, 9th Annual Meeting, p. 1066 (1990).
17. D. B. Twieg, D. J. Meyerhoff, B. Hubesch, K. Roth, D. Sappey-Marinier, M. D. Boska, J. R. Gober, S. Schaefer, and M. W. Weiner, Phosphorus-31 magnetic resonance spectroscopy in humans by spectroscopic imaging: Localized spectroscopy and metabolite imaging, *Magn. Reson. Med.* **12,** 291–305 (1989).
18. A. A. Maudsley, D. B. Tweig, D. Sappey-Marinier, D. Hubesch, J. W. Hugg, G. B. Matson, and M. W. Weiner, Spin-echo ^{31}P spectroscopic imaging of the human brain, *Magn. Reson. Med.* **14,** 415–422 (1990).
19. K. Roth, B. Hubesch, D. J. Meyerhoff, S. Naruse, J. R. Gober, T. J. Lawry, M. D. Boska, G. B. Matson, and M. W. Weiner, Noninvasive quantitation of phosphorus metabolites in human tissue by NMR spectroscopy, *J. Magn. Reson.* **81,** 299–311 (1989).
20. K. O. Lim, J. Pauly, P. Webb, R. Hurd, and A. Macovski, Short TE phosphorus spectroscopy using a spin-echo, *Magn. Reson. Med.* **32,** 98–103 (1994).